Analysis of x-ray emission spectra in charge-exchange collisions of C^{6+} with He and H_2

Anthony C. K. Leung[*] and Tom Kirchner[†]

Department of Physics and Astronomy, York University, Toronto, Ontario, Canada M3J 1P3

(Received 25 March 2016; published 18 May 2016)

Charge exchange in C^{6+}-He and -H_2 collisions followed by x-ray emission is examined using the two-center basis generator method for low to intermediate projectile energies. Within the independent electron model, we calculate capture cross sections and perform a radiative cascade analysis to obtain Lyman line-emission ratios. Single capture is considered for the C^{6+}-He system, while both single capture and autoionizing double capture are considered for the C^{6+}-H_2 system. Effects of a time-dependent screening potential that models target response on the l distribution of capture cross sections and the line-emission ratios are examined as well. Calculated line-emission ratios based on the no-response approximation are in satisfactory agreement with previous measurements.

I. INTRODUCTION

Ever since x-ray and ultraviolet emissions from comets were first observed by Lisse *et al.* [1], numerous theoretical and experimental simulations have been carried out to uncover and understand the process that produces these photoemissions [2–8]. These studies have established that charge exchange (CX) from the comet tail neutral gas to solar wind ions is the production mechanism in essentially all the observed emission lines. Nevertheless, more elaborate and detailed experiments continue to emerge in order to examine x-ray emissions by CX at the quantum level [9–11].

Two experiments performed by Defay *et al.* [12] and Fogle *et al.* [13] at the Oak Ridge National Laboratory (ORNL) multicharged ion research facility measured x-ray emission spectra from CX in C^{6+}-He and -H_2 collisions for energies from 0.5 to 32 keV/amu (corresponding to velocities of approximately 300 to 2500 km/s). At these energies, electron capture is the dominant process. It was found that x-ray emissions in the C^{6+}-He experiment are mainly produced by single-electron capture (SEC), while emissions from C^{6+}-H_2 collisions are produced by SEC and autoionizing double-electron capture (ADC). In both experiments, the C VI Lyman series were resolved using an x-ray quantum calorimeter. Ratios of measured Lyman line emissions were compared with calculated values based on using partial capture cross sections reported in previous studies. Specifically, capture cross sections for the C^{6+}-He system using the atomic-orbital close-coupling (AOCC) [14] and molecular-orbital close-coupling (MOCC) [15] approaches were used in the radiative cascade analysis performed by Defay *et al.* [12]. In addition, Fogle *et al.* [13] reported classical trajectory Monte Carlo (CTMC) calculations for capture in C^{6+}-H_2 collisions. However, since Fogle *et al.* [13] used an *ad hoc* approach for the *nl* population distribution in the radiative cascade calculation, they emphasized the need for other CX models for validation.

In this work, we perform an independent-electron analysis of the x-ray measurements reported in both Refs. [12,13] using the two-center basis generator method (TC-BGM). Previous

TC-BGM calculations were carried out to explain the x-ray spectra from SEC [16] and multiple-electron capture [17] in bare-ion collisions with noble gases. Spectral results obtained from these analyses are in good agreement with experimental measurements. Because these analyses were done for only one collision energy, it is worthwhile to explore the TC-BGM on collision-induced x-ray observations over a range of collision energies. The two collision problems set out by Defay *et al.* [12] and Fogle *et al.* [13] provide an excellent testing ground to examine the applicability and perhaps the limitations of the TC-BGM within the independent electron model (IEM) in explaining the observed x-ray emissions.

First, the TC-BGM and the IEM are described in Sec. II. Calculated ratios of the Lyman emission counts are presented and compared with previous studies in Sec. III. Finally, we provide our concluding remarks in Sec. IV. Atomic units ($\hbar = e = m_e = 4\pi\epsilon_0 = 1$) are used throughout the article unless stated otherwise.

II. THEORETICAL METHOD

A. Collision description

The theoretical calculations for both the C^{6+}-He and -H_2 collision systems are performed within the semiclassical approach where the C^{6+} projectile travels at constant speed v_P in a straight path described by $\mathbf{R}(t) = (b,0,v_P t)$, where b is the impact parameter. Within the IEM, the collision problem is described by the single-particle time-dependent Schrödinger equation (TDSE)

$$i\partial_t \psi_i(\mathbf{r},t) = \hat{h}(t)\psi_i(\mathbf{r},t), \quad i = 1, \dots, N, \quad (1)$$

with the single-particle Hamiltonian

$$\hat{h}(t) = -\frac{1}{2}\Delta - \frac{6}{|\mathbf{r}_P|} + V_T, \quad (2)$$

where $\mathbf{r}_T$ and $\mathbf{r}_P = \mathbf{r}_T - \mathbf{R}(t)$ are the positions of the electron with respect to the target and projectile center, respectively. The effective potential of the target V_T is discussed further below.

The single-particle TDSE (1) is solved using the TC-BGM [18]. The TC-BGM is a coupled-channel method where the single-particle equations (1) are projected onto a finite set of basis states. In this study, the basis set contains the 20

---

[*]leungant@yorku.ca

[†]tomk@yorku.ca

states from the $KLMN$ shells of the target, 56 hydrogenlike states from $n = 1$ to $n = 6$ on the C^{5+} projectile, and 26 BGM pseudostates. The latter are dynamically produced by repeated application of the (regularized) Coulombic projectile potential operator onto atomic target states. This allows convergence to be achieved without resorting to a large basis system, which is the core feature of the TC-BGM [19,20]. The BGM pseudostates account for intermediate quasimolecular couplings and for transitions to the continuum. However, the latter were found to be minor due to the strong dominance of capture transitions in the present study.

Once Eq. (1) is solved we acquire single-particle capture probabilities p^{cap} and target ionization probabilities p^{ion}. They are then combined using multinomial statistics to obtain q-fold capture with simultaneous k-fold ionization P^{qk} [21–23]. Because both helium and molecular hydrogen are two-electron systems, we consider SEC with no ionization

$$P^{10} = 2p^{cap}(1 - p^{cap} - p^{ion})$$ (3)

and double-electron capture (DEC)

$$P^{20} = (p^{cap})^2.$$ (4)

With the combined capture probabilities we calculate capture cross sections

$$\sigma_q^{cap} = 2\pi \int_0^\infty b P^{q0}(b) db, \quad q = 1, 2.$$ (5)

Details regarding the target potential in the single-particle Hamiltonian (2) are described as follows. For the helium target atom, the effective potential, $V_T = V_{He}$, is decomposed as

$$V_{He}(r_T, t) = -\frac{2}{r_T} + v_{ee}(r_T, t),$$ (6)

where

$$v_{ee}(r_T, t) = v_{ee}^0(r_T) + \delta v_{ee}(r_T, t)$$ (7)

is an effective mean-field potential that models the electron-electron interaction on the exchange-only level. We consider two variants: (i) the *no-response* approximation, $\delta v_{ee} = 0$, where the atomic ground-state potential obtained from the optimized potential method of density functional theory [24] is used, and (ii) a *target-response* model, which takes into account a time-dependent screening potential due to electron removal during the collision. The target-response potential is modeled in a global, spherical fashion and was found to have an important role in the low- to intermediate-energy regime in describing capture and ionization [25,26]. Specifically, the response potential of a target with N electrons is taken as [25]

$$\delta v_{ee}(r_T, t) = -\frac{Q_s(t)}{N - 1} v_{ee}^0(r_T),$$ (8)

where for $N = 2$ the time-dependent screening factor assumes the form

$$Q_s(t) = [p_{cap}(t) + p_{ion}(t)]^2.$$ (9)

This screening factor Q_s can be interpreted as the probability for two-electron removal. For $Q_s = 1$, $\delta_{ee} = -v_{ee}^0$ and V_{He} reduces to the Coulomb potential of the target nucleus.

For the H_2 target, we employ the single-center, spherical model potential [27]

$$V_{H_2}(r_T) = -\frac{1}{r_T} - \frac{1}{r_T}(1 + \alpha r_T)e^{-2\alpha r_T},$$ (10)

where $\alpha = 3.93$ is a parameter chosen such that it would yield the correct first ionization energy of the molecule for the fixed internuclear distance of 1.4 a.u. [27]. For this study, we include the target response δv_{ee} to the model potential (10) as well.

The use of model potentials has been a common approach to simplify calculations in atomic and molecular collisions. The model potential for the H_2 molecule (10) has been used previously in Refs. [27,28], where satisfactory results were obtained in estimating cross sections for electron removal and capture at low to intermediate collision energies. In this energy regime, the collision time is considerably shorter than the rotational and vibrational periods of the H_2 molecule. Therefore, it is reasonable to treat these molecular effects as "frozen" during the collisions. In addition, it has been shown in a previous C^{6+}-H_2 collision study that, at low collision energies, capture mainly occurs at $R \approx 8.5$ a.u. for the dominant capture channel [29], which is reasonably far away from the nuclei of H_2 such that the potential can be described using a spherical model.

B. Lyman line emissions

In this study, the main interest is to examine x-ray emissions that correspond to the C VI Lyman series. As we will see in Sec. III, capture mainly occurs in relatively low n states. Therefore, we only consider emissions from Ly-α, -β, and -γ lines.

Using the calculated capture cross sections, we employ the approach by Fogle *et al.* [13] to perform radiative cascade calculations. In this approach, electrons decay to the lowest-energy state following the electric dipole selection rule (i.e., $\Delta l = \pm 1$). If an electron is initially in an excited nl state and decays to a lower-energy state at a rate of $A_{nl \to n'l'}$, then the probabilities of producing Ly-α, -β, and -γ emission lines are

$$P(\text{Ly-}\alpha) = \sigma_2^{rel} s_{2p} + \sigma_3^{rel}(s_{3s} + s_{3d}) + \sigma_4^{rel}\left(s_{4s} \frac{A_{4s \to 2p}}{A_{4s}^{tot}} + s_{4p} \frac{A_{4p \to 3s} + A_{4p \to 3d}}{A_{4p}^{tot}} + s_{4d} \frac{A_{4d \to 2p}}{A_{4s}^{tot}} + s_{4f}\right) + \cdots,$$ (11)

$$P(\text{Ly-}\beta) = \sigma_3^{rel} s_{3p} \frac{A_{3p \to 1s}}{A_{3p}^{tot}} + \sigma_4^{rel}\left(s_{4s} \frac{A_{4s \to 3p}}{A_{4s}^{tot}} \frac{A_{3p \to 1s}}{A_{3p}^{tot}} + s_{4d} \frac{A_{4d \to 3p}}{A_{4d}^{tot}} \frac{A_{3p \to 1s}}{A_{3p}^{tot}}\right) + \cdots,$$ (12)

$$P(\text{Ly-}\gamma) = \sigma_4^{rel} s_{4p} \frac{A_{4p \to 1s}}{A_{4p}^{tot}} + \sigma_5^{rel}\left(s_{5s} \frac{A_{5s \to 4p}}{A_{5s}^{tot}} \frac{A_{4p \to 1s}}{A_{4p}^{tot}} + s_{5d} \frac{A_{5d \to 4p}}{A_{5d}^{tot}} \frac{A_{4p \to 1s}}{A_{4p}^{tot}}\right) + \cdots,$$ (13)

where $\sigma_n^{\text{rel}} = \sigma_n / \sum_i \sigma_i$, $s_{nl} = \sigma_{nl}/\sigma_n$ and $A_{nl}^{\text{tot}} = \sum_{n'l'} A_{nl \to n'l'}$. While this approach has the appeal of avoiding solving the radiative cascade problem using standard rate equations [30,31], the above expressions can get cumbersome if states from higher n levels are included. Regardless, one can view Eqs. (11), (12), and (13) as equivalent representations of the cascade populations obtained from solving the standard rate equations and integrating over time [30].

The radiative decay rates for the singly excited states $A_{nl \to n'l'}$ were calculated using the following expression [16]:

$$A_{nl \to n'l'}^{\text{rad}} = \frac{4}{3} \left(\frac{\omega_{nn'}}{c} \right)^3 (2l'+1) \begin{pmatrix} l' & 1 & l \\ 0 & 0 & 0 \end{pmatrix}^2$$

$$\times \left(\int_0^\infty R_{nl} R_{n'l'} r^3 dr \right)^2, \qquad (14)$$

where $\omega_{nn'}$ is the transition frequency and R_{nl} is the radial wave function for hydrogenlike C^{5+}. Results obtained using Eq. (14) are in excellent agreement with the ones found in OPEN-ADAS [32], which Fogle *et al.* [13] previously used in their radiative cascade calculations.

In the event where ADC contributes to radiative emissions, one needs to include the correct proportion of ADC in the SEC nl cross sections. This can be done by multiplying the DEC cross section by the appropriate branching ratio found from Auger decay rates. In this study, all doubly excited states that undergo Auger processes at some rate W^{Auger} follow the first-order Rydberg cascade. Then, the contribution from all ADC towards some singly excited state nl is

$$\sigma_{nl}^{\text{ADC}} = \sum_{n'l'n''l''} \sigma_{n'l'n''l''} \frac{W_{n'l'n''l'' \to nl}}{W_{n'l'n''l''}^{\text{tot}}}, \qquad (15)$$

where $\sigma_{n'l'n''l''}$ is the DEC cross section and $W_{n'l'n''l''}^{\text{tot}} = \sum_{nl} W_{n'l'n''l'' \to nl}$. The branching ratio defined in Eq. (15) does not include radiative decay rates in doubly excited states. Although x-rays from $(np,n'l') \to (1s,n'l')$ transitions have nearly identical energies to the Lyman line series [11], results from test calculations revealed that Auger rates can be several magnitudes larger than radiative rates for the present problem. In addition, the set of criteria proposed by Ali *et al.* [33] was used to rule out some of the doubly excited states, particularly the highly asymmetrical states (i.e., $n'' \gg n'$), in order to reduce the number of Auger rate calculations.

For the accurate calculation of Auger decay rates, one requires proper descriptions of the bound-state electrons and the outgoing electron to the continuum along with the coupling between these states due to electron-electron interaction. For this study we use the AUGER component of the RATIP program [34] to calculate the Auger rates. The RATIP program provides *ab initio* calculations of the electronic structure and properties of atoms and ions. While RATIP utilizes the multiconfiguration Dirac-Fock method, the present analysis is restricted to single configurations to be consistent with the IEM framework. In the AUGER component, interelectronic interaction is described by instantaneous Coulomb repulsion in the Auger transition amplitude calculation, appropriate for light and medium elements [34]. Moreover, only singlet states are considered in this study since it is unlikely that spin changes

occur during DEC from the singlet He and H_2 ground states [35].

III. RESULTS AND DISCUSSION

A. C^{6+}-He collisions

As a first look at the present results, Fig. 1 shows the SEC probability as a function of impact parameter at $E_P = 1$ keV/amu for the C^{6+}-He collision system. Figures 1(a) and 1(b) show the TC-BGM results based on the no-response approximation and target-response potential, respectively. Both panels show the prominent structure of SEC into $n = 3$ of the C^{5+} projectile. We also see that the capture probabilities in both panels do not exceed 0.5. This reflects the present binomial analysis [see Eq. (3)] provided that ionization is negligible.

There is some noticeable capture into the $n = 4$ channel at small impact parameters seen in Fig. 1. Capture probabilities into other n states are negligibly small at this collision energy (i.e., $< 10^{-6}$); hence, they are not presented in the figure. One interesting difference between the no-response [Fig. 1(a)] and the target-response curves [Fig. 1(b)] is between $b = 1$ and $b = 2$, where the latter result for $n = 4$ is less prominent than the former, but the opposite behavior is seen for $n = 3$. This is a result of the decreased screening of the target core, which
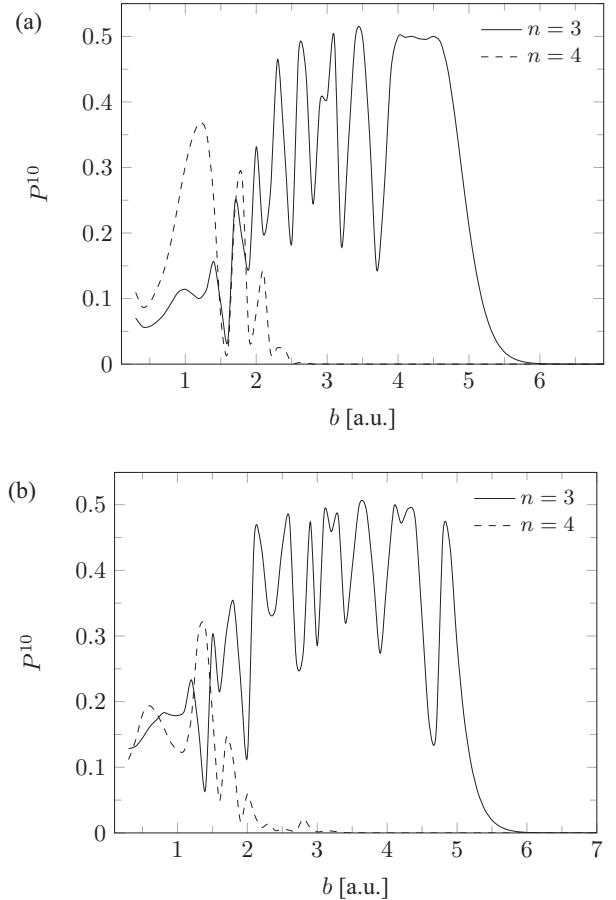
FIG. 1. TC-BGM SEC probabilities plotted with respect to impact parameter for C^{6+}-He collisions at $E_P = 1$ keV/amu. Calculations correspond to (a) the no-response approximation and (b) the target-response model.
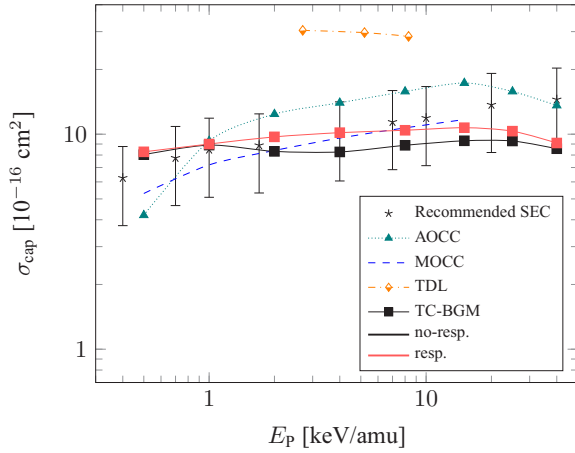
FIG. 2. SEC cross section plotted with respect to collision energy for C^{6+}-He collisions. Calculated SEC values are from AOCC [14], MOCC [15], TDL [36], and the present TC-BGM. Recommended SEC values were compiled by Janev *et al.* [37].

FIG. 3. DEC cross sections plotted with respect to collision energy for C^{6+}-He collisions. Calculations are from the present TC-BGM and OEDM by Harel *et al.* [38]. The combined SEC and DEC cross sections by Harel *et al.* [38] are shown for comparison.

leads to an increased binding of the electron, and so capture into a lower n state is more probable in the target-response model.

To provide credibility to the TC-BGM capture cross sections, it is necessary to compare the present results with existing data from other theoretical and experimental studies. The SEC cross sections for the C^{6+}-He system are shown in Fig. 2 for collision energies from 0.5 to 40 keV/amu. The TC-BGM cross sections are compared with previous SEC calculations, namely, the two-electron calculations based on AOCC [14] and MOCC [15] expansions and the more recent IEM time-dependent lattice (TDL) calculation of Ref. [36]. Because a complete set of measured SEC cross sections in this energy range from a single experiment is not available, we show a compiled list by Janev *et al.* [37] which used Chebyshev polynomial fits on data from various experimental and theoretical studies. The uncertainties of these values were estimated based on the reliability of the experiment and sophistication of the theoretical method [37].

It can be seen that the present SEC cross sections are within the uncertainty range of the recommended values [37]. They are fairly constant between 0.5 and 10 keV/amu before starting to decrease at higher energies. The present cross sections from the no-response and response models are similar across all collision energies. The general discrepancies from the AOCC [14] and MOCC [15] results compared with the present values may be due to several reasons. First, we have to mention that these calculations were performed using two-electron configurations in the wave-function expansion scheme to explicitly describe the interelectronic interaction. This differs from the IEM framework used in the present study where the many-electron processes are described using a multinomial analysis of solutions of the single-particle TDSE.

Another possible explanation for the discrepancies in the cross sections could be the choice of basis. In particular, the helium target basis in the AOCC calculation [14] contained only the ground state. One major concern with having a single state in the target basis is that excitation transitions are blocked, thereby potentially affecting capture transition probabilities.
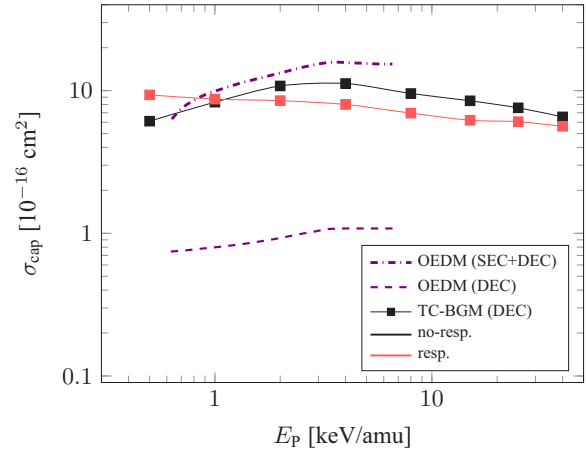
Upon revisiting our TC-BGM calculations, we found that by reducing the target basis only to the ground state we obtained slightly larger cross sections for $E_P > 1$ keV/amu. This could also explain the differences in cross sections between the AOCC [14] and MOCC [15] models since the latter included a $2p$ orbital in addition to $1s$ orbitals in the underlying basis of Slater-type orbitals, which allows for additional dipolelike transitions. However, this did not explain the AOCC cross section at $E_P = 0.5$ keV/amu, leaving the possibility that it may be due to the Coulomb trajectory that was used at $E_P \leqslant 1$ keV/amu [14]. A Coulomb trajectory can yield smaller capture probabilities than a straight-line trajectory, but the magnitude of this effect has not been reported in Ref. [14]. Regardless, the present IEM calculations agree better with AOCC [14] and MOCC [15] than the more recent IEM TDL calculation [36], whose results seem to be too large.

Next, we assess the present DEC cross sections and discuss whether they should be considered in the x-ray analysis via ADC. Defay *et al.* [12] did not consider ADC in describing their x-ray emission measurements, possibly based on the assumption that DEC is negligible. Figure 3 shows the DEC cross sections from the present calculations and results from calculations by Harel *et al.* [38], who used one-electron diatomic molecule (OEDM) orbitals in the expansion scheme with two-electron configurations. The figure also shows the combined SEC and DEC results by Harel *et al.* [38] in order to help gauge the contribution from DEC in the total capture cross section.

Obviously, the present DEC cross sections are much larger than the OEDM results [38]. We note that the OEDM calculation included electron correlations by utilizing an extended Feshbach formalism to obtain a good representation of single- and double-capture channels. Moreover, Harel *et al.* [38] have shown, as an example, that their DEC cross section of the $3l3l'$ state at $E_P = 4.61$ keV/amu ($\sigma_{3l3l'} = 2.1 \times 10^{-17}$ cm^2) is in good agreement with the measurement by Stolterfoht *et al.* [$\sigma_{3l3l'} = (2.4 \pm 0.2) \times 10^{-17}$ cm^2] [39]. Other experiments such as the electron spectroscopy measurement by Mack [40] have shown that the total ADC cross section by L Auger decay

is less than 5×10^{-17} cm^2. From these comparisons it is clear that the present DEC cross sections are overestimated.

Large cross sections from double-electron processes (e.g., capture or ionization) involving a helium target in an IEM calculation have been reported and discussed previously [41–43]. As Singal and Lin [41] suggested, one possible reason for the poor agreement in DEC cross sections from an IEM calculation is that the potential modeled for the helium target does not correspond to the total ionization energy of 2.90 a.u. [44]. In the present study, the potential used for the helium target atom yields the orbital eigenvalue of -0.92 a.u., to be compared with the first ionization potential of 0.90 a.u. [44]. The total ionization energy by the IEM would simply be $2 \times 0.92 = 1.84$ a.u., which is in disagreement with the accepted value [44]. This situation would correspond to our no-response approximation calculation, which would mostly explain how the present SEC cross sections are in good agreement with AOCC [14] and MOCC [15] while DEC is vastly overestimated. To alleviate this issue, Singal and Lin [41] proposed a modified effective potential for the helium target which was modeled such that the binding of each electron is half of the total ionization energy. In the present study within the IEM framework, we approach the double-capture problem by including a target-response potential, but the present results indicate that the model is not adequate to mitigate the issue in a significant way, suggesting that an improved response model is needed.

Another method in working with DEC is the independent *event* model (IEVM) [45]. In this model, a given process is described by a sequence of independent events. In the present framework to describe DEC, this would require calculations of p_{cap} for neutral helium and for the ground-state He$^+$ ion and subsequent multiplication of both. By revisiting our calculation using the IEVM in the no-response approximation, we obtained a DEC cross section of $\sigma_{3l3l'} = 2.2 \times 10^{-17}$ cm^2 at $E_P = 4$ keV/amu, which is consistent with Harel *et al.* [38] and Stolterfoht *et al.* [39]. Since all of these DEC results indicate that the ADC contributions to x-ray emissions should be negligible, there are no additional gains by including them in the present x-ray analysis. Therefore, DEC for the C^{6+}-He system will not be considered further and contributions from pure SEC will be the main focus of discussion.

Figure 4 shows the n-state relative SEC cross-section distributions σ_n^{rel} at collision energies 1, 8, and 25 keV/amu. Results at these energies are selected since, as we will see, they roughly represent the points where noticeable changes in the x-ray measurements occur. We see that the n-state relative populations at each collision energy between no-response and the response model are similar. The plot further illustrates the dominant capture into $n = 3$ of C^{5+} that was discussed earlier (see Fig. 1). This is consistent with AOCC [14], MOCC [15], and the classical over-the-barrier model (CBM) [46,47]. We also observe that the relative population in the dominant capture state ($n = 3$) decreases with increasing energy, leading to a broader distribution. This is consistent with the behavior seen in previous highly charged ion collision studies [48–50].

The weighted nl distributions s_{nl} at projectile energies 1, 8, and 25 keV/amu are shown in Fig. 5. Based on the σ_n^{rel} distribution (Fig. 4), we only show nl populations for $n = 3$ and $n = 4$. For $n = 3$ [Fig. 5(a)], both no-response and target-response
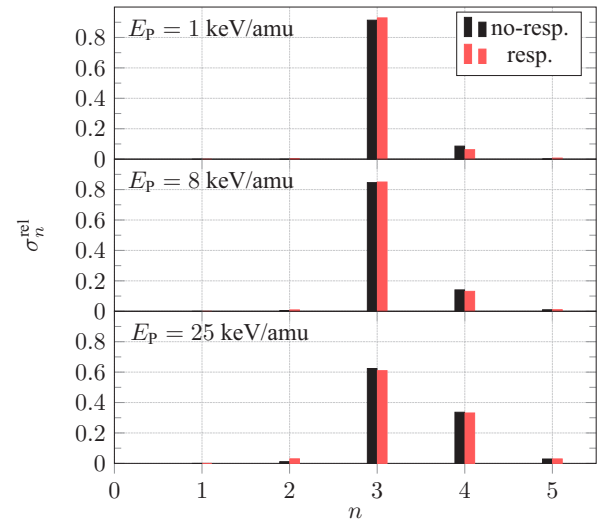

FIG. 4. n-state selective relative SEC cross sections σ_n^{rel} for C^{6+}-He collisions at $E_P = 1$, 8, and 25 keV/amu.
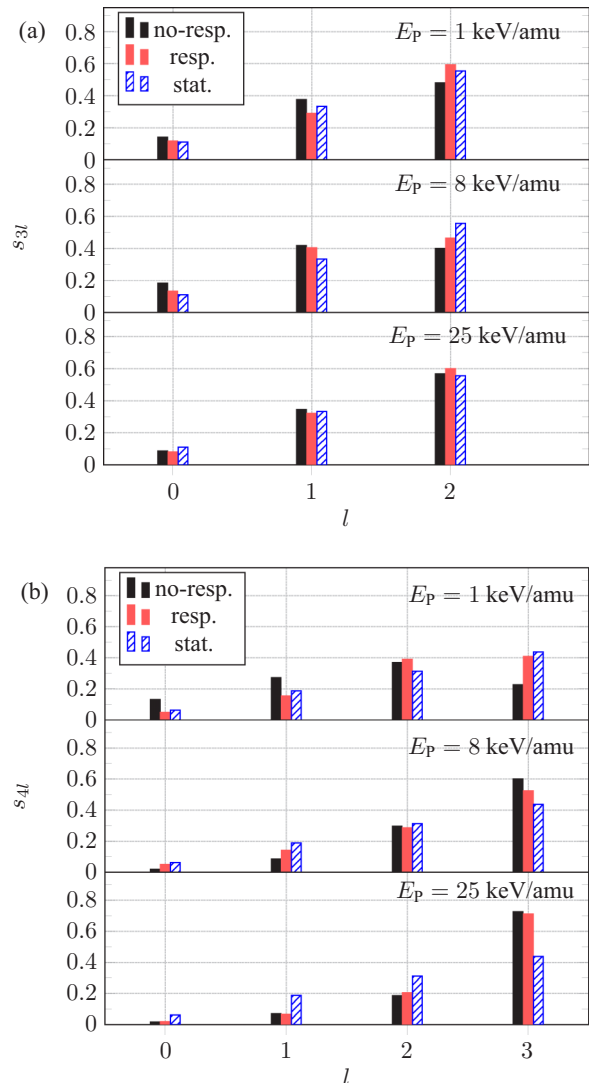

FIG. 5. Weighted partial SEC cross-section distributions s_{nl} for C^{6+}-He collisions at $E_P = 1$, 8, and 25 keV/amu. Distributions correspond to (a) $n = 3$ and (b) $n = 4$.
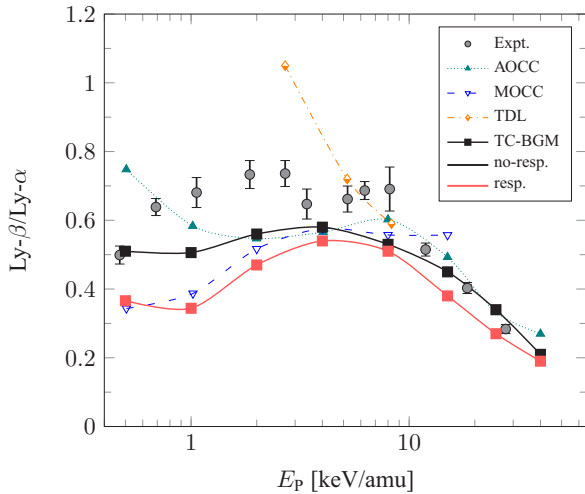
FIG. 6. Ly-β/Ly-α plotted with respect to collision energy for the C^{6+}-He system. Calculated ratios are from the present TC-BGM, AOCC [14], MOCC [15], TDL [36], and measured ratios by Defay *et al.* [12].

FIG. 7. Ly-γ/Ly-α plotted with respect to collision energy for the C^{6+}-He system. Calculated ratios are from the present TC-BGM, AOCC [14], TDL [36], and measured ratios by Defay *et al.* [12].

results exhibit fluctuations in relative population as collision energy increases. We also see that the present $3l$ populations roughly follow the statistical distribution [50] [i.e., $s_{nl} \propto (2l + 1)/n^2$]; hence, we show the latter alongside with the present results for comparison. Moreover, while the relative $3l$ populations between the no-response and target-response calculations differ only slightly at each l state at high collision energies (e.g., at 25 keV/amu), this difference becomes somewhat noticeable at lower energies. Similar observations can be made for the $4l$ distributions [Fig. 5(b)] but with a few exceptions. In particular at $E_P = 1$ keV/amu, the no-response distribution shows that the highest capture probability is in the $l = 2$ state. This differs from the response calculation where the $l = 2$ and $l = 3$ states are approximately populated equally. However, at $E_P = 25$ keV/amu both models agree in that the relative population in all l states is nearly the same and that the population in the $l = 3$ state is substantially higher compared to that in other l states. It is obvious that the statistical distribution is not suitable to describe the $4l$ distribution in this energy regime.

Results of the Lyman emission count ratios, Ly-β/Ly-α, are shown in Fig. 6. The present results are compared with experimental data by Defay *et al.* [12] along with calculated results from AOCC [14], MOCC [15], and TDL [36] models. The experimental ratios are fairly constant between 0.5 and 10 keV/amu before decreasing at $E_P \geqslant 10$ keV/amu. This decreasing trend is attributed to the increased population in the highest l state in both $n = 3$ and $n = 4$ (Fig. 5), which is a significant contributor to Ly-α according to Eq. (11) and also according to the yrast cascade [31] ($\ldots 4f \rightarrow 3d \rightarrow 2p \rightarrow 1s$). We also see that the present response ratios are generally smaller than the no-response results, which can also be explained by the yrast cascade when comparing the highest l-state populations of the calculations (see Fig. 5). Furthermore, ratios from the AOCC [14] and MOCC [15] calculations show trends similar to those of the present results except at and below 1 keV/amu. While TDL ratios at $E_P = 5.20$ and 8.30 keV/amu are on the same level of
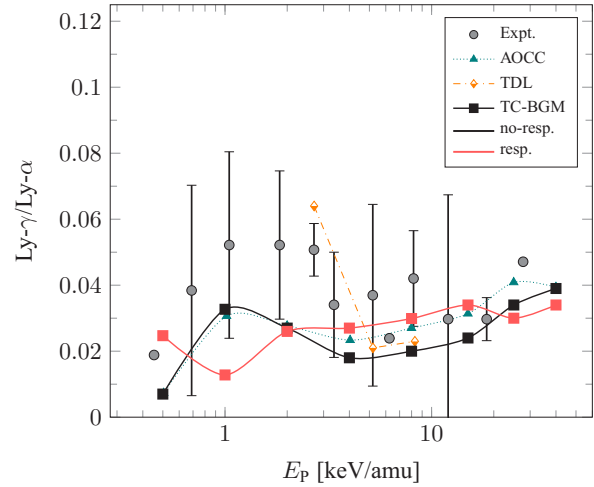
agreement with the experiment, we see that the ratio at 2.70 keV/amu deviates appreciably from the experiment and all other calculations. This is likely due to the substantial difference between the $3p$ and $3d$ cross sections where the relative populations for these states at 2.70 keV/amu were reported to be 57% and 36%, respectively [36]. By Eqs. (11) and (12) the TDL ratio at this collision energy resulted in lower Ly-α but higher Ly-β counts compared to all other calculations.

In Fig. 7, results for the Ly-γ/Ly-α ratios are shown. Cross sections for $n = 4$ were not reported in the MOCC analysis [15], and so ratios from that model cannot be shown. The Ly-γ/Ly-α ratios appear to be smaller in magnitude compared to Ly-β/Ly-α, which is expected given the low Ly-γ counts as a result of small populations in $n \geqslant 4$ shells (see Fig. 4). We also see that the ratios in the no-response and response calculations are similar in magnitude but with slightly different trends. The no-response ratios show a trend that has a closer resemblance to the experiment [12] and AOCC [14]. Moreover, the slightly increasing behavior of the calculated Ly-γ/Ly-α ratios for $E_P \geqslant 10$ keV/amu may be due to the decrease in σ_3^{rel} as collision energy increases (see Fig. 4). As a result, the Ly-α count decreases since Ly-γ does not depend on σ_3^{rel} [see Eq. (13)]. Furthermore, while the TDL ratios [36] are in agreement with the other calculations at $E_P = 5.20$ and 8.30 keV/amu, the ratio at $E_P = 2.70$ keV/amu appears to be closer to the experiment than the other calculations. This could be mainly due to the lower Ly-α count, which is also evident from the Ly-β/Ly-α ratio at this collision energy (Fig. 6). Regardless, without additional data from the TDL calculation [36], it seems difficult to evaluate the overall consistency of that model.

X-ray emissions from CX collisions have been observed to be polarized since magnetic m sublevels are not populated equally in CX processes [51]; hence, one cannot expect the x-ray emission to be isotropic, and comparing calculations that correspond to orientation-integrated measurements with measurements performed at one given orientation is problematic. Nevertheless, if x-rays are detected at a 90° orientation

with respect to the ion beam axis, such as those performed at the ORNL, the errors due to anisotropy can never be larger than 30%, provided that the x-rays are fully polarized [52]. Furthermore, previous experiments have shown that errors of 15% or lower are typically observed [3,53]. By inspecting the experimental error bars reported by Defay *et al.* [12], it is not absolutely certain if errors due to polarization are taken into account. From this, if we consider the upper limit of 15% in addition to the experimental errors reported by Defay *et al.* [12], then we would consider the present calculations in the no-response approximation to be in acceptable agreement with the experimental ratios. The response model produces similar trends but somewhat less satisfactory agreement with the experimental data.

B. C^{6+}-H_2 collisions

An example of the TC-BGM results for SEC probabilities for the C^{6+}-H_2 collision system is shown in Fig. 8 at $E_P = 1$ keV/amu, separated by no response [Fig. 8(a)] and target response [Fig. 8(b)]. The probability curves show that $n = 4$ is the dominant capture channel and capture mainly takes place at $b \leqslant 9$. As previously discussed for the C^{6+}-He system (Fig. 1), capture probabilities into the $n = 3$ shell at small impact
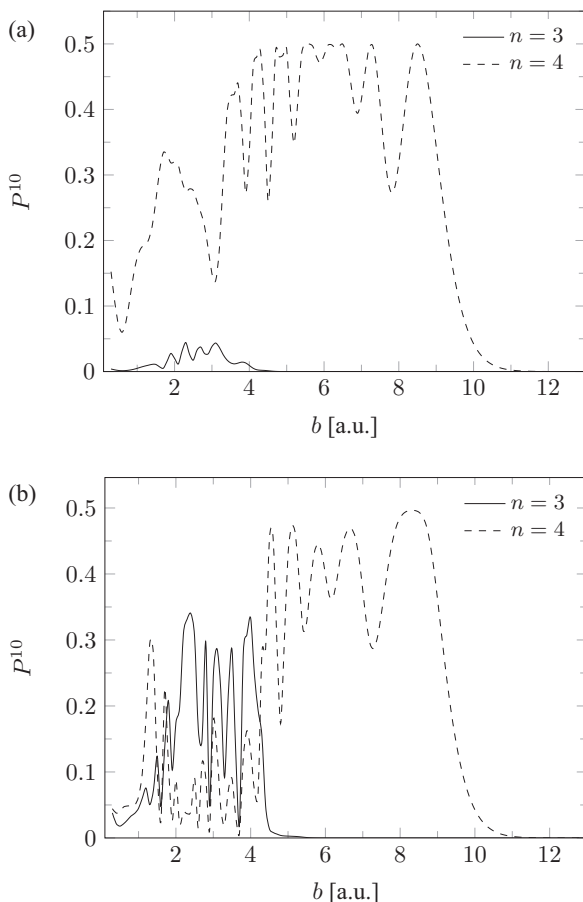

(a)

(b)

FIG. 8. TC-BGM SEC probabilities plotted with respect to impact parameter for C^{6+}-H_2 collisions at $E_P = 1$ keV/amu. Calculations correspond to (a) the no-response approximation and (b) the target-response model.

TABLE I. Capture cross sections (in 10^{-16} cm^2) in C^{6+}-H_2 collisions at $E_P = 4$ keV/amu. Calculated values are from TC-BGM in the no-response and response models; experimental data are from Hoekstra *et al.* [53] and Mack [40].

	No response	Response	Hoekstra *et al.* [53]	Mack [40]
σ_{SEC} ($n = 3$)	2.67	3.73	3 ± 2	
σ_{SEC} ($n = 4$)	25.99	22.58	32 ± 8	
σ_{SEC} ($n = 5$)	1.56	0.94	1.5 ± 1	
σ_{ADC}	15.58	15.09	11 ± 4	12.3

parameters are smaller in the no-response approximation than the response curve, but the opposite tendency is seen for the $n = 4$ channel. This is consistent with the effects from the increased binding by the target nucleus as described by the target-response potential. It can also be seen in both panels that the capture probabilities in the most probable state (i.e., $n = 4$) do not exceed the 0.5 limit of the IEM framework.

Next, we assess the present total capture cross sections by comparing them with results from previous studies. Table I lists the experimental capture cross sections at $E_P \approx 4$ keV/amu by Mack [40] and Hoekstra *et al.* [53], along with the present TC-BGM calculations. We first see that the present cross sections from the response model are generally smaller than those of the no-response approximation except for SEC at $n = 3$. Unlike for the C^{6+}-He system, it has been shown in electron spectroscopy measurements [40] that production of C^{5+} in C^{6+}-H_2 collisions from ADC is not negligible. This can be seen in Table I. The experimental ADC cross section by Hoekstra *et al.* [53] is similar to the measurement by Mack [40], and they are comparable to the SEC value for $n = 4$. We also see that the present cross sections by both models are mostly close to the experimental measurements. The exception that is shown is the present SEC cross section for $n = 4$, which is slightly underestimated compared to the result by Hoekstra *et al.* [53]. This can be understood by the limitation of the present IEM analysis, as discussed earlier (see Fig. 8).

In another comparison, Fig. 9 shows the total SEC cross sections with respect to collision energy from the present calculations, two-electron MOCC calculations by Kimura [29], and measurements by Meyer *et al.* [54]. Because Meyer *et al.* [54] could not distinguish SEC and ADC in their measurements, we can infer that these measurements correspond to the sum of SEC and ADC processes. To demonstrate this with the present results, we show the pure SEC and the combined SEC+ADC cross sections separately in Fig. 9. From this we see that the latter results agree very well with the experimental data [54], particularly the response results. However, we also see in Fig. 9 that the results from the full two-electron MOCC calculation by Kimura [29], which only included SEC channels, are closer to Meyer *et al.* [54] than the present SEC results. This inconsistency between the present SEC+ADC results and the MOCC-SEC results could be related to basis-set convergence issues in the latter analysis since that work was not aimed at precision. In fact, Kimura stated that a larger basis-set calculation could change the two-electron MOCC-SEC results by, at most, 30% [29].
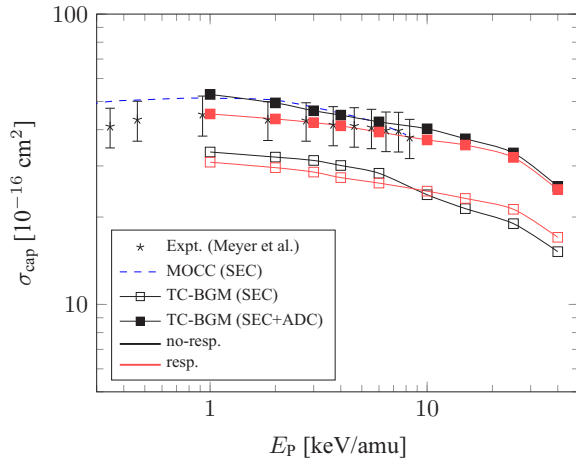
FIG. 9. Capture cross sections plotted with respect to collision energy for C^{6+}-H_2 collisions. Experimental values are from Meyer *et al.* [54], shown along with the present TC-BGM results and MOCC calculations [29].

FIG. 10. n-state selective relative SEC and SEC+ADC cross sections σ_n^{rel} for C^{6+}-H_2 collisions at $E_P = 1$, 6, and 25 keV/amu.

In Sec. III A, it was shown how the present DEC cross sections for the C^{6+}-He system were in poor agreement with previous calculations and experiments. However, the situation is different for the C^{6+}-H_2 system, although both were analyzed within the IEM framework. This can be understood with the same argument regarding the total ionization energy of the target. Despite both helium and H_2 being two-electron systems, the total electronic energy of the latter is -1.16 a.u. [55]. In the present study, the potential used for H_2 yields an energy eigenvalue of -0.60 a.u., whose magnitude is close to the accepted first ionization potential of 0.57 a.u. [55]. Therefore, one can see that the total ionization energy by the IEM (1.20 a.u.) is close to the accepted value (1.16 a.u.) [55]. We recall that Singal and Lin [41] have shown that if an effective potential of a two-electron target is constructed such that the binding of each electron is half of the total ionization energy, then the DEC cross sections would result in closer agreement with the experiment. This would explain how the IEM framework, in particular with the response model, is shown to be more successful in describing DEC for the H_2 target than for helium. From this discussion and the explicit checks with previous results, there is enough confidence that the present ADC results can be considered further in the x-ray analysis.

Figure 10 shows the present σ_n^{rel} distributions due to SEC and the combined SEC+ADC processes at $E_P = 1$, 6, and 25 keV/amu. Based on the measurements by Fogle *et al.* [13], considerable changes in x-ray ratios can be seen at these collision energies. In the SEC distributions, the dominant capture channel of $n = 4$ can be seen at all collision energies. This is consistent with the SEC cross sections by Hoekstra *et al.* [53] and with the CBM. Similar to the C^{6+}-He case, the n distribution of the capture cross section broadens as collision energy increases. Minor differences in relative populations can be seen between the no-response and response models across all n states. We also see that including contributions from ADC results in a substantial increase in population in the $n = 2$ and $n = 3$ states. Upon review of the Auger decay calculations, we
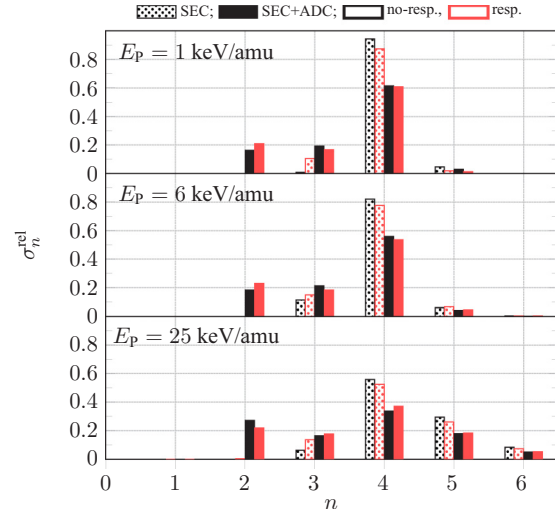
found contributions towards final states of $n \geqslant 4$ from ADC to be negligible.

The weighted nl distributions are presented in Fig. 11. We show distributions within the $n = 2$ [Fig. 11(a)], $n = 3$ [Fig. 11(b)], and $n = 4$ shells [Fig. 11(c)]. As mentioned previously, contributions from ADC in $n = 4$ are negligible, and therefore, only populations by SEC are shown in Fig. 11(c). We note that the CTMC calculation by Fogle *et al.* [13] assumed a statistical distribution for the l-state population in the low-energy regime, while an overstatistical model was used in the intermediate regime. Therefore, we show and compare the weighted statistical distribution alongside the present results. Generally speaking, the SEC nl distributions from the response model have a closer resemblance to the statistical distribution than the no-response results. However, the statistical model appears inadequate at 25 keV/amu to describe the $4l$ distribution [Fig. 11(c)] since the population in $l = 3$ is substantially larger than that in the lower l states. Furthermore, things look different when ADC is included in addition to SEC. For example, the $2l$ distributions [Fig. 11(a)] now resemble an even (flat) distribution. Noticeable changes can also be seen in the $3l$ distributions [Fig. 11(b)], where both no-response and response results closely follow the statistical distribution.

Figure 12 displays the Ly-β/Ly-α ratios for C^{6+}-H_2 collisions. The figure shows emission ratios resulting from both SEC and the combined SEC+ADC processes. We compare the present ratios based on the no-response and target-response calculations with measurements and CTMC calculations by Fogle *et al.* [13]. When examining the SEC ratios, we see that the present results follow closely the experimental trend. We note that, as mentioned by Fogle *et al.* [13], the noticeable deviation of the experimental ratio at $E_P \approx 3.5$ keV/amu could be due to a systematic error that was not taken into account.

Within the target-response model, the Ly-β/Ly-α ratios by SEC appear to reach a maximum at around 6 keV/amu. The maximum is mostly attributed to the decreasing $3d$ and $4f$ populations between 1 and 6 keV/amu before increasing again
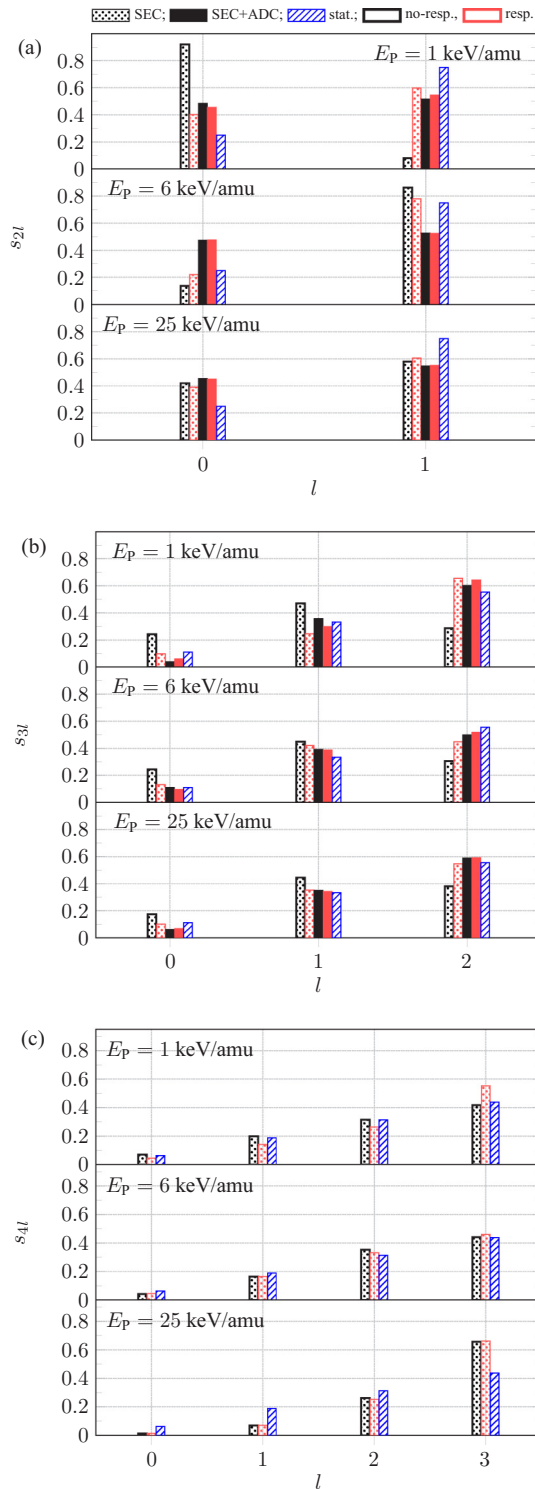
FIG. 11. Weighted partial SEC and SEC+ADC cross-section distributions s_{nl} for C^{6+}-H_2 collisions at 1, 6, and 25 keV/amu. Distributions correspond to (a) $n = 2$, (b) $n = 3$, and (c) $n = 4$.

at higher energies [see Figs. 11(b) and 11(c)]. The changes in Ly-α counts would reflect the changes in those populations if the yrast cascade is followed. As for the no-response case, the ratios between 1 and 6 keV/amu appear fairly constant before decreasing at higher energies. While the no-response
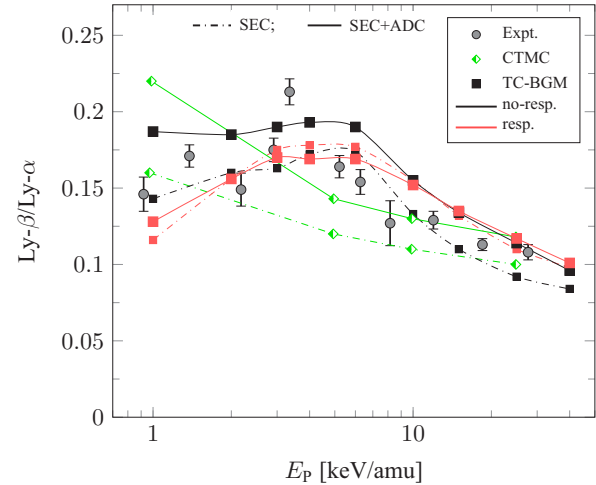

FIG. 12. Ly-β/Ly-α plotted with respect to collision energy for the C^{6+}-H_2 system. Experimental ratios are by Fogle *et al.* [13]. Calculated ratios are from CTMC [13] and TC-BGM from SEC and SEC+ADC cross sections.

and response ratios are similar at 2 to 10 keV/amu, noticeable differences can be seen at higher energies. This may be due to the different relative population in the $n = 5$ state (see Fig. 10), where the relative population in the no-response approximation is slightly larger than the population in the response model.

By including contributions from ADC, we see an overall increase in the Ly-β/Ly-α ratios in the no-response case while retaining the general trend from SEC, a tendency that can also be seen in the CTMC ratios [13]. As for the response ratios, including contributions from ADC does not show significant changes despite seeing changes in the relative populations (Fig. 11). This implies that changes in the Ly-α and -β counts are proportional.

The Ly-γ/Ly-α ratios are shown in Fig. 13. The ratios show a decreasing trend with respect to collision energy. From the
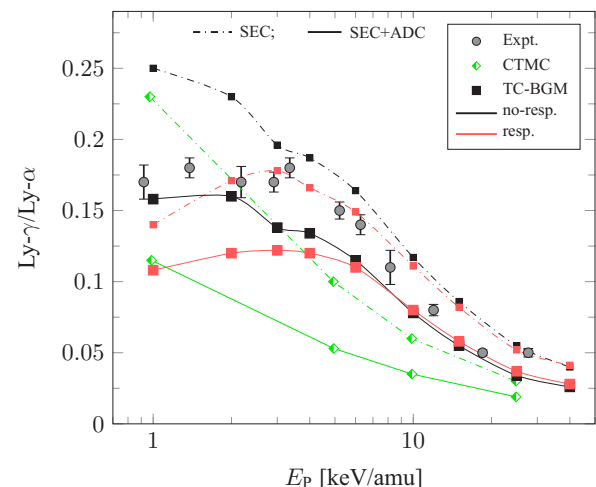

FIG. 13. Ly-γ/Ly-α plotted with respect to collision energy for the C^{6+}-H_2 system. Experimental ratios are by Fogle *et al.* [13]. Calculated ratios are from CTMC [13] and TC-BGM from SEC and SEC+ADC cross sections.

SEC results between $E_P = 1$ and 6 keV/amu the TC-BGM ratios from the target-response calculation are closer to the experimental ratios than the no-response approximation and CTMC. One can also see that the no-response and target-response ratios converge as energy increases. By including contributions from ADC, the emission ratios decrease while maintaining the same general trend seen in the SEC ratios. It can be seen that the present no-response ratios are now closer to the experiment than the response ratios. Recall that only Auger decays with $n = 2$ and $n = 3$ final states are seen, which explains the lower ratios from the increased Ly-α counts but no changes in Ly-γ. Moreover, the CTMC ratios also show a decrease when ADC is taken into account, but the difference between these ratios and the experiment is more pronounced. Clearly, taking the ADC contributions into account has a noticeable influence on the level of agreement or disagreement of the calculations with the experimental data.

The overall discrepancies seen between the present and the CTMC ratios is at least partially due to the reliance on the *ad hoc* distribution that Fogle *et al.* [13] used to estimate the nl population in the CTMC calculation. As seen from the present nl distributions, the populations change with respect to collision energy, and the line-emission ratios can reflect those changes in a noticeable way. Moreover, while the target-response model has provided an improved total capture cross section (Fig. 9), it does not result in an improved estimation of the x-ray ratios. Overall, by also taking into account the uncertainties of the x-ray measurements due to polarization, we find the present x-ray results satisfactory.

IV. CONCLUSIONS

We have carried out an independent-electron analysis of x-ray emissions from CX in C^{6+}-He and -H_2 collisions at low to intermediate energies using the TC-BGM. Capture cross sections were obtained by solving the single-particle TDSE and were then used in a radiative cascade model to obtain x-ray emission probabilities that correspond to the Lyman line series. From these two collision studies, additional insights were gained about the TC-BGM in terms of its capabilities to describe collision-induced radiation emissions and the use of model potentials within the IEM framework.

In the analysis of C^{6+}-He collisions, the TC-BGM cross sections for SEC were considered in the Lyman line-emission calculations. Results for the Ly-β/Ly-α and Ly-γ/Ly-α ratios in the no-response approximation showed satisfactory agreement with measurements by Defay *et al.* [12]. Moreover, we showed how emission ratios vary with collision energy by looking at the nl-state population distributions. While previous studies have suggested that contributions from ADC are negligible for the observed x-ray emissions, the present calculation was not able to verify these measurements. Specifically, the

present DEC cross sections were found to be overestimated, which is mainly due to the inability of the helium potential used to describe the correct energy needed for removing both electrons [41]. Although a response model that includes a time-dependent screening of the helium target was used, it did not provide significant improvements on the DEC cross sections.

In the analysis of C^{6+}-H_2 collisions, we employed a single-center, spherical model potential to describe the molecular target in the TDSE calculations. Results for both SEC and ADC cross sections using this potential led to very good agreement with measurements by Meyer *et al.* [54], Mack [40], and Hoekstra *et al.* [53]. Overall, the present calculations of the Lyman line-emission ratios are in satisfactory agreement with measurements by Fogle *et al.* [13]. Furthermore, the present results show that the nl cross sections in the dominant n state mainly follow the statistical distribution in the low-energy regime, while an overstatistical model is better suited in the intermediate regime, confirming some of the predictions made by Fogle *et al.* [13]. However, the subdominant capture states may not necessarily follow these distributions strictly, as shown by the present results. Therefore, reliance on an *ad hoc l* distribution is not recommended for radiative cascade calculations.

Another important insight gained from this study is the level of accuracy of the target-response potential for describing collision-induced radiative emissions. While the target-response potential has provided an improved estimation of total SEC cross sections in the low-energy regime, the present x-ray results indicate that this model does not provide an improved estimation of *partial* cross sections. Specifically, it was found that the present response potential has the tendency to yield a higher relative population in the maximum l state than the no-response approximation, which mostly led to the discrepancies seen with the experimental emission ratios in both collision systems. Therefore, there is an impelling reason to investigate for an improved target-response model that would resolve these issues.

[1] C. M. Lisse, K. Dennerl, J. Englhauser, M. Harden, F. E. Marshall, M. J. Mumma, R. Petre, J. P. Pye, M. J. Ricketts, J. Schmitt, J. Trumper, and R. G. West, Science **274**, 205 (1996).

[2] T. E. Cravens, Geophys. Res. Lett. **24**, 105 (1997).

[3] J. B. Greenwood, I. D. Williams, S. J. Smith, and A. Chutjian, Phys. Rev. A **63**, 062707 (2001).

[4] P. Beiersdorfer, R. E. Olson, G. V. Brown, H. Chen, C. L. Harris, P. A. Neill, L. Schweikhard, S. B. Utter, and K. Widmann, Phys. Rev. Lett. **85**, 5090 (2000).

[5] P. Beiersdorfer, M. Bitter, M. Marion, and R. E. Olson, Phys. Rev. A **72**, 032725 (2005).

[6] R. Ali, P. A. Neill, P. Beiersdorfer, C. L. Harris, M. J. Raković, J. G. Wang, D. R. Schultz, and P. C. Stancil, Astrophys. J. **629**, L125 (2005).

[7] F. I. Allen, C. Biedermann, R. Radtke, G. Fussmann, and S. Fritzsche, Phys. Rev. A **78**, 032705 (2008).

[8] P. Beiersdorfer, L. Schweikhard, P. Liebisch, and G. V. Brown, Astrophys. J. **672**, 726 (2008).

[9] R. Ali, P. A. Neill, P. Beiersdorfer, C. L. Harris, D. R. Schultz, and P. C. Stancil, Astrophys. J. **716**, L95 (2010).

[10] M. Trassinelli, C. Prigent, E. Lamour, F. Mezdari, J. Mérot, R. Reuschl, J. Rozet, S. Steydli, and D. Vernhet, J. Phys. B **45**, 085202 (2012).

[11] R. Ali, P. Beiersdorfer, C. L. Harris, and P. A. Neill, Phys. Rev. A **93**, 012711 (2016).

[12] X. Defay, K. Morgan, D. McCammon, D. Wulf, V. M. Andrianarijaona, M. Fogle, D. G. Seely, I. N. Draganić, and C. C. Havener, Phys. Rev. A **88**, 052702 (2013).

[13] M. Fogle, D. Wulf, K. Morgan, D. McCammon, D. G. Seely, I. N. Draganić, and C. C. Havener, Phys. Rev. A **89**, 042705 (2014).

[14] W. Fritsch and C. D. Lin, J. Phys. B **19**, 2683 (1986).

[15] M. Kimura and R. E. Olson, J. Phys. B **17**, L713 (1984).

[16] A. C. K. Leung and T. Kirchner, Phys. Rev. A **92**, 032712 (2015).

[17] A. Salehzadeh and T. Kirchner, J. Phys. B **46**, 025201 (2013).

[18] M. Zapukhlyak, T. Kirchner, H. J. Lüdde, S. Knoop, R. Morgenstern, and R. Hoekstra, J. Phys. B **38**, 2353 (2005).

[19] H. J. Lüdde, A. Henne, T. Kirchner, and R. M. Dreizler, J. Phys. B **29**, 4423 (1996).

[20] O. J. Kroneisen, H. J. Lüdde, T. Kirchner, and R. M. Dreizler, J. Phys. A **32**, 2141 (1999).

[21] D. R. Schultz, R. E. Olson, C. O. Reinhold, S. Kelbch, C. Kelbch, H. Schmidt-Böcking, and J. Ullrich, J. Phys. B **23**, 3839 (1990).

[22] M. Horbatsch, Phys. Rev. A **49**, 4556 (1994).

[23] T. Kirchner, H. J. Lüdde, and R. M. Dreizler, Phys. Scr., T **80**, 416 (1999).

[24] E. Engel and S. H. Vosko, Phys. Rev. A **47**, 2800 (1993).

[25] T. Kirchner, M. Horbatsch, H. J. Lüdde, and R. M. Dreizler, Phys. Rev. A **62**, 042704 (2000).

[26] T. Kirchner, M. Horbatsch, and H. J. Lüdde, Phys. Rev. A **66**, 052719 (2002).

[27] L. F. Errea, J. D. Gorfinkiel, C. Harel, H. Jouin, A. Macías, L. Méndez, B. Pons, and A. Riera, J. Phys. B **33**, 3107 (2000).

[28] D. Elizaga, L. F. Errea, J. D. Gorfinkiel, C. Illescas, L. Méndez, A. Macías, A. Riera, A. Rojas, O. J. Kroneisen, T. Kirchner, H. J. Lüdde, A. Henne, and R. M. Dreizler, J. Phys. B **32**, 857 (1999).

[29] M. Kimura, Phys. Rev. A **33**, 4440 (1986).

[30] L. J. Curtis, Am. J. Phys. **36**, 1123 (1968).

[31] S. M. Younger and W. L. Wiese, Phys. Rev. A **17**, 1944 (1978).

[32] OPEN-ADAS, http://open.adas.ac.uk/.

[33] R. Ali, C. L. Cocke, M. L. A. Raphaelian, and M. Stockli, Phys. Rev. A **49**, 3586 (1994).

[34] S. Fritzsche, J. Electron Spectrosc. Relat. Phenom. **114–116**, 1155 (2001).

[35] M. Mack, J. H. Nijland, P. v. d. Straten, A. Niehaus, and R. Morgenstern, Phys. Rev. A **39**, 3846 (1989).

[36] M. S. Pindzola and M. Fogle, J. Phys. B **48**, 205203 (2015).

[37] R. Janev, R. Phaneuf, and H. Hunter, At. Data Nucl. Data Tables **40**, 249 (1988).

[38] C. Harel, H. Jouin, and B. Pons, J. Phys. B **24**, L425 (1991).

[39] N. Stolterfoht, K. Sommer, J. K. Swenson, C. C. Havener, and F. W. Meyer, Phys. Rev. A **42**, 5396 (1990).

[40] M. Mack, Nucl. Instrum. Methods Phys. Res., Sect. B **23**, 74 (1987).

[41] R. Singal and C. D. Lin, J. Phys. B **24**, 251 (1991).

[42] Y. D. Wang, C. D. Lin, N. Toshima, and Z. Chen, Phys. Rev. A **52**, 2852 (1995).

[43] M. McCartney, J. Phys. B **30**, L155 (1997).

[44] *CRC Handbook of Chemistry and Physics*, 96th ed., edited by W. M. Haynes (CRC Press, Boca Raton, FL, 2015), pp. 197–199.

[45] K. M. Dunseath and F. Crothers, J. Phys. B **24**, 5003 (1991).

[46] H. Ryufuku, K. Sasaki, and T. Watanabe, Phys. Rev. A **21**, 745 (1980).

[47] A. Niehaus, J. Phys. B **19**, 2925 (1986).

[48] H. Ryufuku and T. Watanabe, Phys. Rev. A **20**, 1828 (1979).

[49] R. E. Olson, Phys. Rev. A **24**, 1726 (1981).

[50] R. Janev and H. Winter, Phys. Rep. **117**, 265 (1985).

[51] D. Vernhet, A. Chetioui, K. Wohrer, J. P. Rozet, P. Piquemal, D. Hitz, S. Dousson, A. Salin, and C. Stephan, Phys. Rev. A **32**, 1256 (1985).

[52] D. Dijkkamp, Y. S. Gordeev, A. Brazuk, A. G. Drentje, and F. J. de Heer, J. Phys. B **18**, 737 (1985).

[53] R. Hoekstra, D. Ciric, F. J. de Heer, and R. Morgenstern, Phys. Scr. T **28**, 81 (1989).

[54] F. W. Meyer, A. M. Howald, C. C. Havener, and R. A. Phaneuf, Phys. Rev. A **32**, 3310 (1985).

[55] D. Sprecher, C. Jungen, W. Ubachs, and F. Merkt, Faraday Discuss. **150**, 51 (2011).